Journal of Cultural Heritage 71 (2025) 203–210

Contents lists available at ScienceDirect

Journal of Cultural Heritage

journal homepage: www.elsevier.com/locate/culher

Original article

The effect of organosilicon compounds on the nanostructure of waterlogged archeological oak studied by neutron and X-ray scattering

Nayomi Z. Plaza[a], Sai Venkatesh Pingali[b], Magdalena Broda[c,*]

[a] Forest Products Laboratory, Forest Service, United States Department of Agriculture, Madison, WI 53726, USA
[b] Neutron Scattering Division, Oak Ridge National Laboratory, Oak Ridge, TN 37831, USA
[c] Department of Wood Science and Thermal Techniques, Faculty of Forestry and Wood Technology, Poznan University of Life Sciences, ul. Wojska Polskiego 38/42, 60-637 Poznan, Poland

ARTICLE INFO

Article history:
Received 4 October 2024
Accepted 29 November 2024

Keywords:
Waterlogged wood
Archeological wood
Nanoscale
Organosilicon compounds
Silane
Siloxane
Microfibril
SANS
SAXS
WAXS

ABSTRACT

Selected organosilicon compounds proved effective in stabilizing waterlogged wood dimensions upon drying. However, detailed knowledge about their effect on wood is necessary before introducing them as safe waterlogged wood consolidants in conservation practice. Our previous research showed that organosilicons can chemically react with wood polymers, infiltrate cell walls and/or fill cell lumina. These interactions can mechanically reinforce the cell wall or have a plasticizing effect on wood, depending on the compound applied. To better understand their stabilizing effect on waterlogged wood, we used neutron and X-ray scattering methods, which enabled us to study the nanostructure of archeological oak wood and recognize if and how treatment with selected organosilicon compounds modified it. The results showed that archeological wood had a reduced amount of crystalline cellulose and a less ordered nanostructure with larger elementary fibrils that are more loosely packed compared to sound wood. X-ray and neutron scattering also revealed that applied alkoxysilanes restored the long-range cellulose arrangement in archaeological oak samples to different extents, whereas siloxane did not. This restoration was visible in increased anisotropy in the SAXS/SANS patterns and increased intensity in the WAXS data. The most effective silane treatment restored both SAXS/SANS and WAXS features. Combining the macroscale characterization of treated and untreated archaeological oak with the X-ray and neutron scattering work suggests that the nanoscale changes in the cell wall imparted by the infiltration of selected organosilicons contribute to the increased dimensional stability of archeological wood treated with these compounds.

1. Introduction

Stabilizing agents used for waterlogged wood conservation should primarily ensure its integrity and dimensional stabilization upon drying because degraded wood tissue saturated with water is particularly prone to shrinking, cracking, and disintegrating when excavated and exposed to air-drying unprotected [1–3]. In addition to historical alum treatment that proved detrimental to historical wood in the long term [4–7], polyethylene glycols and multiple sugars have been commonly used in conservation practice but are not free from flaws [8–14]. Thus, the search for a perfect consolidant for waterlogged wood continues. Several agents have been explored, including cellulose and lignin derivatives [15–19], various natural polysaccharides [1,17,19,20], Halloysite nanotubes in combination with wax, esterified colophony, and pluronic block copolymer [21–24], proteins [25–28], reversibly cross-linked polymers [29], and other chemicals [30–37], some of which can also be applied for direct in situ underwater wood consolidation.

In our previous research, we observed that a wide range of organosilicon compounds had promising results with regard to stabilizing efficacy and potential use in the conservation of waterlogged wooden artifacts [38–40]. However, since their stabilizing effectiveness differed depending not only on the individual chemical structure and properties of the compound but also on the chemical composition, species, and degradation degree of the treated wood [38–43], we performed a thorough study to explain the mechanism of wood stabilization by organosilicon compounds. We analyzed the reactivity of individual organosilicons with wood, their deposition within the wood structure, as well as their effects on the wood mechanical properties at the nanoscale (cell walls) and macroscale (whole wooden blocks) [40,41,43–45]. We learned that organosilicons could interact with the hydroxyl groups on the

* Corresponding author.
E-mail address: magdalena.broda@up.poznan.pl (M. Broda).

https://doi.org/10.1016/j.culher.2024.11.021

wood polymers, infiltrate cell walls and/or locate in cell lumina, mechanically reinforce the cell wall, or have a plasticizing effect on the wood, depending on the agent applied. However, it remains unclear whether these chemicals alter the wood nanostructure and whether these changes contribute to wood's dimensional stabilization.

Among the best techniques to study the inner structure of the wood cell wall at the nanometer scale are neutron and X-ray scattering methods. With minimum sample preparation, they enable the observation of nanoscale structures in a macroscopic sample under both dry and wet conditions [46–48]. Small-angle neutron scattering (SANS), along with small- and wide-angle X-ray scattering (SAXS and WAXS), have proven particularly useful in measuring the average size and spacing of cellulose elementary fibrils in sound and untreated wood [48–53], investigating moisture-induced structural changes in the wood nanostructure [48,54–58], as well as studying nanoscale changes in the wood cell wall caused by various treatments and modifications, including propylene oxide, butylene oxide, and acetic anhydride [59], phenol-formaldehyde [55], polymethylmethacrylate [60] and polyethyleneglycol [9,49]. These techniques have also been used to investigate alterations in the wood nanostructure caused by fungal decay [44,46,47], as well as analyze the degradation of archeological wood on the nanometer scale [9,61–63].

2. Research aim

Here, we used SANS, SAXS, and WAXS to recognize the changes in the archeological oak wood nanostructure caused by hundreds of years of natural degradation under waterlogged conditions compared with sound contemporary wood. Moreover, we aimed to determine if and how treatment with selected organosilicon compounds modify the nanostructure of waterlogged archeological wood to evaluate if the nanoscale changes contribute to the observed wood dimensional stabilization. The knowledge gained from the study will help better understand the mechanism of wood dimensional stabilization by these chemicals and contribute to developing new effective agents for waterlogged wood conservation.

3. Materials and methods

3.1. Research material

This study was conducted using an archeological oak wood (*Quercus robur* L.) log excavated from the basement of the Psalteria building at Ostrow Tumski (Cathedral Island) in Poznan (the Wielkopolska Region, Poland). Buried in wet soil for over 1000 years, it was once one of the construction elements of wooden city walls surrounding the medieval early Piast settlement [64]. The wooden tissue was relatively well preserved, with a loss of wood substance estimated at about 10% [65], and filled with water, so it was a suitable material for research on new agents for waterlogged wood conservation. Contemporary oak of the same species was purchased from commercial timber merchants in the Wielkopolska Region, Poland.

The middle part of the log was cut into small blocks with dimensions of 20 × 20 × 10 mm (radial x tangential x longitudinal direction). The specimens used for the study were sampled one after the other to ensure as much homogeneity as possible. They all had similar density, which translates to a similar degree of degradation, which is vital for obtaining reliable results when testing different conservation agents. Such samples were then treated with 50% solutions of three different organosilicon compounds in 96% ethanol. The selected organosilicons were Methyltrimethoxysilane (MTMOS), (3-Mercaptopropyl)trimethoxysilane (MPTMOS), and 1,3-Bis-[(diethylamino)-3-(propoxy)propan-2-ol]-1,1,3,3-tetramethyldisiloxane (DEAPTMDS), which have already proven effective in stabilizing wood dimensions [38,39]. Oak wood samples treated with the organosilicons were named O1, O2, and O3, respectively. Wood impregnation was conducted using the oscillating vacuum-pressure method, as previously described [41]. Part of the wood samples remained untreated and served as a control. To assess the stabilizing effect of organosilicons on waterlogged wood, bulk density, bulk wood weight percent gain, volumetric shrinkage, and volumetric anti-shrink efficiency coefficient were calculated for all samples after air-drying, as described in our previous work [41]. The results obtained are presented in Table 1.

Table 1
Bulk density (ρ), bulk wood weight percent gain (WPG_{BW}), volumetric shrinkage (S_v), and volumetric anti-shrink efficiency (ASE_v) for archeological oak wood – untreated (Oc), treated with Methyltrimethoxysilane (O1), treated with (3-Mercaptopropyl)trimethoxysilane (O2), and treated with 1,3-Bis-[(diethylamino)-3-(propoxy)propan-2-ol]-1,1,3,3-tetramethyldisiloxane (O3) [41]; ± standard deviations.

Sample ID	ρ (g cm^{-3})	WPG_{BW} (%)	S_v (%)	ASE_v (%)
Oc	0.46±0.03	–	6.5 ± 0.4	–
O1	0.60±0.03	22.4 ± 3.1	2.5 ± 1.2	61.2
O2	0.63±0.02	30.7 ± 4.2	4.2 ± 1.4	35.9
O3	0.59±0.06	30.8 ± 2.2	2.9 ± 1.3	55.4

3.2. Sample preparation

Radial-longitudinal sections (0.7 mm thick) were cut from air-dried untreated and treated oak wood blocks with a razor blade. Some sections were then soaked overnight in D_2O and used for SANS measurements, while others were used for WAXS/SAXS measurements at dry conditions.

3.3. Small-angle neutron scattering (SANS)

Thin radial-longitudinal sections were immersed in D_2O using titanium cells with a 1 mm spacer, as described before [66]. Air bubbles were removed, and the cells were refilled with D_2O if needed. SANS measurements were performed at the BioSANS instrument at the High Flux Isotope Reactor facility at the Oak Ridge National Laboratory [67], using the dual-detector configuration to achieve a q-range of 0.003 – 0.85 Å^{-1}. An incident wavelength of 6 Å and a sample aperture of 14 mm were used.

Data were corrected for background, pixel sensitivity, and dark current, normalized by monitor counts, then anisotropically reduced using the drt-sans reduction package [68]. The equatorial SANS data were modeled in the IRENA package [69] to track the changes in the small angle diffraction peak position (q_0) and, consequently, the elementary fibril spacing ($EFs_N = 2\pi/q_0$) using the following equation:

$$\boldsymbol{I(q) = B_1 q^{-P_1} + B_2 q^{-P_2} + A e^{\frac{-(q-q_0)^2}{2w^2}} + B_3} \quad (1)$$

where P_1 and P_2 are the low-q and mid-q power law exponents, respectively, and B_1 and B_2 are the power law prefactors. The diffraction peak is described by a Gaussian peak with amplitude A, centered at q_0 and width w. B_3 is a constant background. A second small angle diffraction peak was observed for treated samples; thus, another Gaussian peak with peak position q_m, as well as variable width and amplitude, were added. The corresponding real-space dimension (d_m) was calculated as 2π /q_m.

3.4. Wide- and small-angle X-ray scattering (WAXS/SAXS)

Radial-longitudinal thin sections were taped onto a flat plate holder and measured in both WAXS and SAXS configurations using

a Xeuss 3.0 by Xenocs (Grenoble, France) X-ray scattering system equipped with a Ga metal jet source and an Eiger Dectris 2D detector array [66]. A broad range of scattering vectors (q) was acquired, ranging from 0.0035 to 3.4 $Å^{-1}$. Each sample was measured for 300 s under vacuum to reduce air scattering contributions. A spot size of 0.5 mm was used for all measurements.

Data were integrated into equatorial and meridional sectors using the NIKA package [70] based on IgorPro 9 macros (WaveMetrics, Lake Oswego, OR, USA), and the meridional data were subtracted from the equatorial ones. Typically, a total width of 24° was used for each sector. To enhance the small-angle diffraction peak position q_x, scattering intensity I(q) was plotted using a Kratky plot $q^2I(q)$ vs. q, fitted with a Gaussian, and the elementary fibril spacing was determined ($EFs_X = 2\pi/q_x$). The elementary fibril diameter (EF_{dia}) was determined from the minimum in the SAXS curve [71] by fitting the SAXS curve (0.09 $Å^{-1}$ < q < 0.7 $Å^{-1}$) to Eq. (2), which includes a constant background B, a prefactor I_0, and a Bessel function of the first kind (J_1):

$$\boldsymbol{I}(\boldsymbol{q}) \approx I_0\left(4\frac{J_1\left(\frac{q}{2}EF_{dia}\right)}{qEF_{dia}}\right)^2 + B \quad (2)$$

WAXS data were also modeled using a polynomial background and four pseudo-Voigt peaks (one for each cellulose Iβ diffraction peak, (i.e., the 200, the 004, and the doublets (110 and 1–10)). The peak positions (q_{hkl}) were then used to calculate the distance between planes (d_{hkl}) using $d_{hkl} = 2\pi/q_{hkl}$. To determine a degree of restoration ($A_{200}/A_{200\ CO}$), we tracked the area under the 200-peak for each sample and normalized it with respect to the one obtained for contemporary wood. All fits to the X-ray scattering data were done in Python using the lmfit library [72].

4. Results

The differences between degraded archeological and sound contemporary oak wood and the effects of organosilicon treatment on archeological oak in the SANS patterns are shown in Fig. 1a. For contemporary oak (CO) soaked in D_2O, there is a diamond-shaped scattering pattern at the low-q and a diffraction peak in the high-q regime. These characteristic features are still present in all the archeological oak samples, but the anisotropy is less pronounced compared to the contemporary wood. This indicates that the long-range spatial architecture of cellulose in the cell wall of archeological wood has been degraded, which suggests some extent of wood degradation.

The equatorial scattering profiles for all samples are shown in Fig. 1b. For contemporary wood, there are two power laws and a distinct diffraction peak (q~0.17 $Å^{-1}$), from which we can calculate the center-to-center distance between elementary fibrils (EFs_N). Whereas the untreated archeological wood sample (Oc) has a less pronounced peak that is shifted to lower q (from 0.17 $Å^{-1}$ to 0.12 $Å^{-1}$). The high-q diffraction peak is also present in organosilicon-infiltrated samples but is shifted towards higher q (~0.13 $Å^{-1}$) than the untreated Oc. The treated samples also have a weak mid-q diffraction peak (q~0.05$Å^{-1}$), which is most noticeable for O2 (Fig. 1c). Here, we use the term elementary fibril to name a universal structural unit of cellulose, whose cross-section is about 2–3 nm [71,73–75]. Elementary fibrils aggregate into bundles called microfibrils [76].

Parameters obtained from fitting the SANS data to the Eq. (1) are listed in Table 2. The scattering power law observed in the low-q ($q < 0.01\ Å^{-1}$) is similar for all samples. In the mid-q ($0.01\ Å^{-1} < q < 0.08\ Å^{-1}$), there is an increase in the exponent for archeological samples compared to the contemporary wood sample. Scattering from rods yields a power law exponent of −1, whereas scattering from discs, lamellae, or Gaussian polymer chains could result in exponents of −2 [77]. An increase in the mid-q power law would suggest that the wood polymers (such as the elementary fibrils) are more flexible and have more random conformations in degraded samples. Similar mid-q power laws have been reported for pine modified with alkylene oxides, and some also exhibited a mid-q shoulder feature [78]. The mid-q peak observed in treated samples is similar for all and corresponds to a characteristic dimension of 12 nm. It is unclear what structural organization could be giving rise to this feature in the scattering profile. Microfibrils (their size and arrangement in the cell wall) could contribute to the scattering in this q-range, but the contrast in unmodified wood is typically not favorable for resolving these characteristic features. It is possible that the treated samples have enhanced contrast and/or the scattering contribution from the microfibrils has increased due to the treatment – if some of the polymer particles infiltrated this region (and we have already shown that the applied organosilicons can infiltrate the cell wall [41]), it is possible that their contrast with respect to the microfibrils is better than the contrast between the wood polymers. In the high-q, the archeological sample has increased EFs_N (Oc is 40% higher than CO). It indicates a loosened structure of cellulose microfibrils in the Oc sample that is more susceptible to moisture-induced swelling compared to sound CO, confirming some extent of degradation of archeological wood. Treated archeological samples have lower EFs_N compared to the untreated Oc, but the spacings are still larger than those of the contemporary oak. This confirms some degradation of archeological wood but also indicates that the treatment affected its nanostructure – possibly organosilicon particles infiltrated the degraded microfibril structure, somewhat templating the cellulose arrangement and thus pre-swelled the microfibrils when compared to contemporary wood structure, but made their structure more compact than in the untreated degraded Oc sample.

Table 2
SANS fitted parameters for sound contemporary oak (CO) and archeological oak untreated (Oc) and infiltrated with selected organosilicons: Methyltrimethoxysilane (O1), (3-Mercaptopropyl)trimethoxysilane (O2), and 1,3-Bis-[(diethylamino)-3-(propoxy)propan-2-ol]-1,1,3,3-tetramethyldisiloxane (O3) included the power law exponents (P_1 and P_2) and the characteristic dimensions obtained from the mid-q and high-q peaks, d_m and EFs_N. Uncertainties due to data variations (shown in parenthesis) were estimated by adding Gaussian noise and evaluating its effect. The values for untreated archeological wood marked with asterisks have higher uncertainties compared to other samples.

Sample ID	Low q	Mid q		High q
	$q < 0.01\ Å^{-1}$	$0.01\ Å^{-1} < q < 0.08\ Å^{-1}$		$q > 0.08\ Å^{-1}$
	P_1	P_2	d_m (nm)	EFs_N (nm)
CO	3.75 (0.001)	1.4 (0.010)	–	3.75 (0.01)
Oc	4.16 (0.01)*	1.8 (0.044)	–	5.28 (0.8)*
O1	3.95 (0.001)	1.7 (0.004)	11.8 (0.05)	4.68 (0.02)
O2	3.96 (0.001)	1.9 (0.003)	12.5 (0.15)	5.06 (0.05)
O3	3.83 (0.001)	1.8 (0.004)	12.8 (0.07)	5.45 (0.02)

Small-angle and wide-angle X-ray scattering (SAXS and WAXS) from archeological untreated and treated oak samples are shown in Fig. 2. Data for contemporary oak (CO) is also included as a reference. Scattering from the archeological untreated sample is much more isotropic than contemporary oak (Fig. 2a). Treated samples (O1 and O2) also display anisotropic scattering, with O2 being the most anisotropic. Considering that all samples had similar thicknesses and were carefully prepared with the same primary orientation with respect to the X-ray beam, this indicates that these treatments are helping restore some of the anisotropy lost due to the wood degradation and that MPTMOS is the most effective in this regard.

Azimuthally integrated scattering profiles are shown in Fig. 2b. The packing of the elementary fibrils contributes to the shoulder seen in the SAXS data (q~0.15 $Å^{-1}$), which decreases in intensity for the archeological samples, confirming some degree of wood

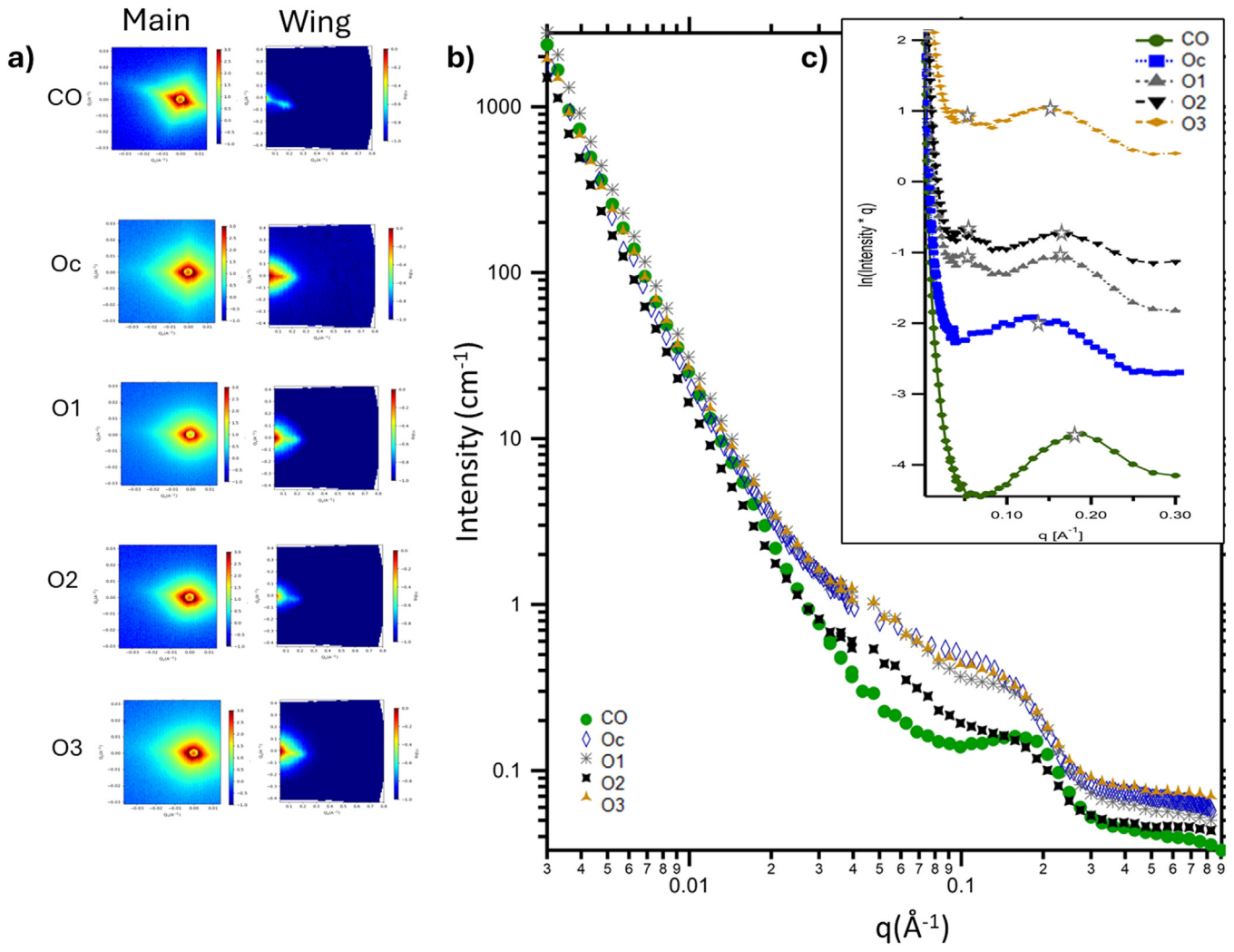

Fig. 1. SANS anisotropic scattering patterns from archeological oak untreated (Oc) and infiltrated with selected organosilicons: Methyltrimethoxysilane (O1), (3-Mercaptopropyl)trimethoxysilane (O2), and 1,3-Bis-[(diethylamino)-3-(propoxy)propan-2-ol]-1,1,3,3-tetramethyldisiloxane (O3) obtained with the (a) main and (b) wing detectors. Equatorial scattering profiles are shown in (b). Diffraction peaks in the high-q and mid-q are identified with stars (c), and a shift towards lower q in the high-q peak indicates an increase in the elementary fibril spacing. Data for contemporary oak (CO) is also included for reference.

degradation. The minimum in the SAXS curves (q ~0.3 $Å^{-1}$), from which the diameter of the elementary fibrils can be estimated [71], is visually similar for all samples except for the most severely degraded ones.The decrease in the structure factor contribution is enhanced in the Kratky plot (Fig. 2c). For the untreated Oc sample, the small-angle peak is barely noticeable compared to the contemporary sample, whereas for the treated samples, the peak is partially restored and has been shifted towards lower q. In the WAXS region (Fig. 2d), all samples have the signature diffraction peaks of cellulose Iβ (200, 1–10/110, and the 004), but the intensity of these peaks is reduced in the archeological samples compared to the contemporary one. The data presented above indicate that archeological wood was degraded to some extent compared to contemporary wood and that the applied organosilicon treatments restored the intensity of the characteristic diffraction peaks to different degrees, where MPTMOS was the most effective one.

All structural parameters obtained from fitting the SAXS and WAXS data in this study are listed in Table 3. Most archeological samples have slightly increased elementary fibril diameters (EF_{dia}) and spacings (EFs_X) compared to the contemporary oak (CO), which agrees with the trends observed via SANS. The distances between diffraction planes increased for 200 and 004, whereas there is no trend in the doublet region. Overall, the intensity of the WAXS diffraction peaks decreased in all archeological samples to different degrees compared to CO. Interestingly, O2 is the only one that has restored both the overall WAXS signal and the nanoscale structure as evidenced by the similarities in the parameters from SAXS and WAXS. It should be noted that organosilicons in the cell wall could contribute to the WAXS scattering, and we expect these contributions to be isotropic, but it is possible that they are also contributing to the increase in intensity observed in the treated samples. To compare the effects of treatment in the WAXS signal, we tracked the ratio of the area under the 200 peak for the archeological samples with respect to the contemporary oak to define a degree of restoration ($\frac{A_{200}}{A_{200CO}}$). This parameter would vary between 0 and 1, with 1 corresponding to a perfectly restored structure that is similar to contemporary undegraded wood. Most archeological samples had similar degrees of restoration despite the treatment, and only O2 showed a substantial degree of restoration (0.87 vs 0.44). It should be noted that variations in thickness, primary orientation, or acquisition time could impact the WAXS signal used to define the restoration parameter. So, in this study, all these variables were kept constant to minimize variabilities that could hinder relative comparisons.

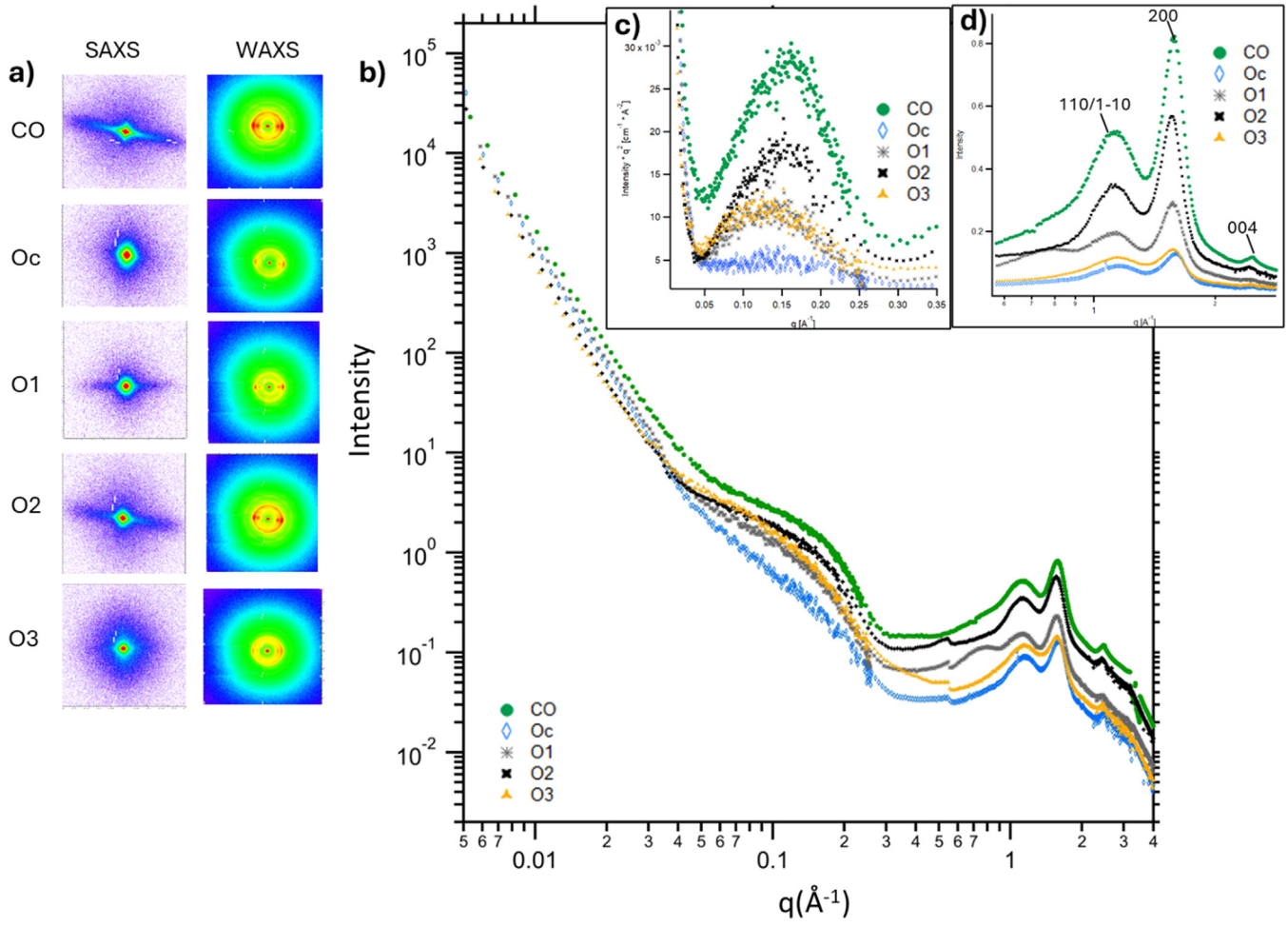

Fig. 2. X-ray scattering of contemporary oak (CO) and archeological oak untreated (Oc) and infiltrated with selected organosilicons: Methyltrimethoxysilane (O1), (3-Mercaptopropyl)trimethoxysilane (O2), and 1,3-Bis-[(diethylamino)-3-(propoxy)propan-2-ol]-1,1,3,3-tetramethyldisiloxane (O3). Loss of anisotropic features is observed in both (a) small and wide-angle X-ray 2D scattering patterns. (b) Equatorial scattering profiles (corrected for isotropic contributions by subtracting the meridional data) showing the SAXS shoulder (q~0.15 Å^{-1}) and the SAXS minimum (q~0.3 Å^{-1}). The small angle diffraction peak contribution is enhanced in (c). The WAXS region (d) exhibits all characteristic peaks for cellulose Iβ (i.e., 200, 004, and 110/1–10), but the intensities are greatly reduced for the untreated archeological oak (Oc). Organosilicon treatments restore long-range order as evidenced by the increase in the small angle due to the elementary fibrils (c) and the WAXS 200 diffraction peak (d).

Table 3
Parameters obtained for contemporary oak (CO) and archeological oak untreated (Oc) and infiltrated with selected organosilicons: Methyltrimethoxysilane (O1), (3-Mercaptopropyl)trimethoxysilane (O2), and 1,3-Bis-[(diethylamino)-3-(propoxy)propan-2-ol]-1,1,3,3-tetramethyldisiloxane (O3) from fitting the X-ray scattering data. SAXS was used to measure elementary fibril diameter (EF_{dia}), and spacings (EFs_X) and distances between diffraction planes (d200 and d004) were determined from WAXS. Uncertainties from least square fits are shown in parenthesis.

Sample ID	SAXS		WAXS				
	EFs_X (nm)	EF_{dia} (nm)	d_{200} (Å)	d_{004} (Å)	d_{110} (Å)	d_{1-10} (Å)	$\frac{A_{200}}{A_{200\,CO}}$
CO	4.2 (0.1)	2.5 (0.3)	3.98 (0.01)	2.50 (0.08)	5.22 (0.04)	5.85 (0.03)	1.00
Oc	4.9 (0.1)	2.9 (0.1)	4.00 (0.06)	2.55 (0.01)	5.15 (0.01)	5.79 (0.01)	0.44
O1	4.7 (0.2)	2.8 (0.2)	4.02 (0.03)	2.57 (0.01)	5.39 (0.20)	5.90 (0.66)	0.44
O2	4.2 (0.2)	2.5 (0.1)	4.04 (0.01)	2.58 (0.01)	5.23 (0.10)	5.80 (0.05)	0.87
O3	4.9 (0.1)	2.9 (0.2)	4.04 (0.08)	2.57 (0.02)	5.15 (0.01)	5.84 (0.15)	0.35

5. Discussion

Characterization of archeological oak samples with neutron and X-ray scattering methods helped understand the changes in the wood nanostructure caused by natural decay during its burial under waterlogged conditions for hundreds of years. Despite a relatively low degree of wood degradation (wood mass loss estimated at about 10% [65]), the obtained results showed that compared to sound oak, the archeological untreated one has a less ordered nanostructure with larger elementary fibrils (EF_{dia}) that are more loosely packed (17% EFs_X and 41% EFs_N larger values than Oc). At the molecular level, WAXS revealed larger spacings between the cellulose 200 diffraction planes and a 56% loss of the peak intensity, indicating a reduction in the amount of crystalline cellulose in the sample. WAXS intensities and eventual loss of reflections have also been observed by other researchers for various kinds of archeological wood [62,79,80]. Previous investigations on severely deteriorated wood (both archaeological and model-degraded) have also exhibited more isotropic SAXS signals, which have been attributed to an overall increase in nanoscale porosity and more disordered microfibrils [61,62,66].

Combining the results of the X-ray and neutron scattering work with macroscale characterization of treated archaeological wood performed in our previous research [38,40,41,44] helped to bet-

ter understand how organosilicons affect wood treated with these compounds and how the imparted changes can contribute to its increased dimensional stability.

Our previous synchrotron-based X-ray fluorescence microscopy (XFM) studies have shown that all three organosilicons used in the study can infiltrate wood cell walls, and while MTMOS and MPTMOS had comparable levels of infiltration (3–4%), that of BDEAPPTMDS was larger (~ 7%), and this chemical also filled cell lumina [41]. X-ray and neutron scattering revealed that among used organosilicons, alkoxysilanes (MTMOS and MPTMOS) were able to restore the long-range cellulose arrangement in the archaeological oak samples to different extents, whereas siloxane (DEAPTMDS) was not. This restoration was visible in three ways: (1) increased anisotropy in the SAXS/SANS patterns, (2) increased intensity in the SAXS shoulder or SANS peak, and (3) increased intensity in the cellulose 200 peak. The most effective treatment (MPTMOS) was able to restore all three. Although it did not directly translate to the highest dimensional stabilization of slightly degraded oak wood treated with this silane (Table 1), it is worth mentioning here, that MPTMOS was the most effective in stabilizing dimensions of highly degraded waterlogged elm wood (reaching ASE of about 98%) [38,40].

Scattering studies showed that organosilicon infiltration modified the packing of the elementary fibrils (EFs_X) and their moisture-induced swelling (EFs_N). Alkoxysilanes (MTMOS and MPTMOS) decreased the disorder imparted by wood degradation and decreased the nanoscale swelling observed for untreated archeological wood, with MPTMOS being the most effective in both measures. Conversely, the siloxane did not change the packing of the elementary fibrils in O3 samples but allowed a 3% increase in nanoscale swelling. These differences between alkoxysilanes and siloxane likely arise from how these compounds interact with the wood polymers. FT-IR and NMR studies on treated highly degraded archeological elm have shown that both MTMOS and MPTMOS can interact with wood polysaccharides and lignin, with MPTMOS forming apparent new chemical bonds with cellulose, while DEAPTMDS just modifies polysaccharides and lignin, including α-decarboxylation and demethoxylation of its aromatic units, and forming mainly hydrogen bonds with wood polymers [40,44]. Thus, the combination of strong chemical interaction with both cellulose and lignin is the most beneficial with regards to restoring the long-range order in the nanostructure as well as imparting dimensional stability. The improved long-range order of the cellulose is also likely to reinforce the structural integrity of the degraded cell wall and its mechanical properties, which is consistent with previous nanoindentation studies [41].

The combined results of our studies on organosilicon compounds used for waterlogged wood conservation clearly show that the mechanism of wood dimensional stabilization by these chemicals is complex and depends on many variables, including the type of wood species, wood anatomical structure, chemical composition and degree of its degradation, as well as molecular weight, chemical structure, and resulting properties and reactivity of applied organosilicon compounds [38,40,41,43,44]. It seems that in the case of slightly degraded archaeological oak, the infiltration of the wood structure, including both infiltration of cell walls and filling cell lumina, provided by DEAPTMDS, worked better in stabilizing wood dimensions than the reinforcement of the structure and mechanical properties of degraded cell wall provided by alkoxysilanes MTMOS and MPTMOS [41]. However, we should remember that the archeological oak used for the study was only slightly degraded. Therefore, the WPG of all organosilicons was low, so the plasticizing effect of DEAPTMDS was not as apparent as we observed in the case of more degraded wood [43]. The calculated shrinkage values were also low and had relatively high standard deviations compared to the shrinkage values themselves. Hence, the differences between individual organosilicons' effectiveness were not statistically important. In the case of more degraded archeological elm wood and model degraded pine wood, the most effective was the treatment with MPTMOS, followed by DEAPTMDS and MTMOS in the case of elm wood and chemically degraded pine or by MTMOS and DEAPTMDS for biologically degraded pine [38,40,43]. As our extensive studies show, the factors that contribute to the exceptional ability of MPTMOS to stabilize wood dimensions include (1) relatively small molecular mass and size of its particles, allowing it to penetrate the wood cell wall nanostructure, (2) the presence of alkoxy groups that react chemically with wood polymers and other silane monomers through covalent bonds forming a 3D polymer network inside the wood structure, and (3) the presence of additional reactive mercapto groups capable of forming even stronger covalent bonds with wood polymers [38,44]. As a result, MPTMOS infiltrates the degraded wooden cell walls, reinforcing their nanostructure and mechanical properties, thus providing dimensional stabilization crucial to keeping the size and shape of a waterlogged wooden artifact during drying. MTMOS treatment seems to work similarly, except for the absence of strong chemical bonds with wood polymers through additional reactive functional groups, which apparently are essential to provide the cell walls with enough strength to keep wood dimensions almost intact [39,44]. In the case of siloxane DEAPTMDS, the stabilizing mechanism seems different. The molecules of the organosilicon are bigger and devoid of chemical groups that could form chemical bonds with wood, creating a stable polymer network inside the wood structure [40,44]. Although siloxane can infiltrate the cell walls, it does not restore its degraded nanostructure. Moreover, it has a plasticizing effect on wood on the nano- and macroscale since it remains not fully polymerized due to the absence of reactive groups forming covalent bonds [43,81,82]. However, infiltrating cell walls and filling cell lumina, plus the formation of hydrogen bonds with wood polymers, seems to be sufficient to effectively stabilize the dimensions of waterlogged wood during drying.

6. Conclusions

X-ray and neutron scattering measurements of untreated and treated archeological wood demonstrated changes in the wood nanostructure caused by natural degradation during centuries of its burial under waterlogged conditions. They also revealed how the applied organosilicon compounds used for wood impregnation affected its degraded nanostructure. Alkoxysilanes Methyltrimethoxysilane and (3-Mercaptopropyl)trimethoxysilane restored the long-range cellulose arrangement in the archaeological oak samples to different extents, with the latter being more effective, whereas a siloxane 1,3-Bis-[(diethylamino)-3-(propoxy)propan-2-ol]-1,1,3,3-tetramethyldisiloxane did not do that.

Combining the results of our previous macroscale characterization of treated and untreated archaeological wood with the X-ray and neutron scattering work has shown that the nanoscale changes imparted by the infiltration of organosilicons in the cell wall can help explain the mechanisms behind their improved dimensional stabilization effectiveness. They helped recognize two different stabilizing mechanisms depending on the type and chemical structure of applied organosilicons:

- alkoxysilanes infiltrate the cell walls and react strongly with wood polymers, restoring the cell wall nanostructure and reinforcing its mechanical properties, thus stabilizing the dimensions of waterlogged wood during drying,
- siloxane interacts with wood polymers only through weak hydrogen bonds, infiltrates cell walls, and fills cell lumina; its stabilizing effectiveness apparently comes mainly from filling cavities in degraded wood, thus helping withstand capillary forces of evaporating water during drying.

A general conclusion from our research is that organosilicon treatment, although effective in stabilizing waterlogged wood dimensions, cannot be considered universal since its effectiveness depends on the type and properties of both an applied chemical and treated wood. Therefore, as usual in the conservation practice, a specific conservation approach should be developed depending on the needs of a particular wooden artifact.

Revealing the complexity and individual components of the stabilizing mechanism of organosilicon compounds on wood constitutes an important step on the road to designing conservation agents tailored to the needs of individual wooden artifacts of cultural heritage.

Acknowledgments

The research was supported by the Polish-U.S. Fulbright Commission through a Fulbright Senior Award 2020/21 granted to Magdalena Broda. A portion of this work acknowledges the support of the Genomic Science Program, Office of Biological and Environmental Research (OBER), U.S. Department of Energy (DOE), under Contract FWP ERKP752. The SANS studies on Bio-SANS were supported by the OBER funding Center for Structural Molecular Biology (CSMB) under Contract FWP ERKP291, using the High Flux Isotope Reactor supported by the Basic Energy Sciences, Department of Energy. Access to the Xeuss 3 SAXS/WAXS instrument was obtained via the ORNL instrumentation pool. The Xeuss 3 instrument was funded via the ORNL LDRD program. The findings and conclusions in this publication are those of the authors and should not be construed to represent any official USDA or U.S. Government determination or policy. This manuscript has been coauthored by UT-Battelle, LLC, under Contract No. DE-AC05- 00OR22725 with the U.S. Department of Energy. The United States Government retains and the publisher, by accepting the article for publication, acknowledges that the United States Government retains a non-exclusive, paid-up, irrevocable, worldwide license to publish or reproduce the published form of this manuscript or allow others to do so, for United States Government purposes.

References

[1] M. Broda, C.A. Hill, Conservation of waterlogged wood—past, present and future perspectives, Forests 12 (2021) 1193, doi:10.3390/f12091193.
[2] D.W. Grattan, R.W. Clarke, 9 - Conservation of waterlogged wood, in: C. Pearson (Ed.), Conservation of Marine Archaeological Objects, Butterworth-Heinemann, Oxford, 1987, pp. 164–206, doi:10.1016/B978-0-408-10668-9.50015-0.
[3] D. Grattan, M. Bilz, T. Grant, J. Logan, Outcome determines treatment – an approach to the treatment of waterlogged wood, J. Wetl. Archaeol. 6 (2006) 49–63, doi:10.1179/jwa.2006.6.1.49.
[4] S. Braovac, C.M.A. McQueen, M. Sahlstedt, H. Kutzke, J.J. Łucejko, T. Klokkernes, Navigating conservation strategies: linking material research on alum-treated wood from the Oseberg collection to conservation decisions, Herit. Sci. 6 (2018) 77, doi:10.1186/s40494-018-0241-y.
[5] S. Braovac, H. Kutzke, The presence of sulfuric acid in alum-conserved wood–Origin and consequences, J. Cult. Herit. 13 (2012) S203–S208, doi:10.1016/j.culher.2012.02.002.
[6] C.M.A. McQueen, M.N. Mortensen, F. Caruso, S. Mantellato, S. Braovac, Oxidative degradation of archaeological wood and the effect of alum, iron and calcium salts, Herit. Sci. 8 (2020) 32, doi:10.1186/s40494-020-00377-0.
[7] C.M. McQueen, J.J. Lucejko, I.M. Flaate, F. Modugno, S. Braovac, Ammonium alum in alum-treated wooden artefacts: discovery, origins and consequences, Herit. Sci. 7 (2019) 1–11, doi:10.1186/s40494-019-0321-7.
[8] A. Vorobyev, G. Almkvist, N.P. van Dijk, E.K. Gamstedt, Relations of density, polyethylene glycol treatment and moisture content with stiffness properties of Vasa oak samples, Holzforschung 71 (2017) 327–335, doi:10.1515/hf-2016-0202.
[9] L. Wagner, G. Almkvist, T.K. Bader, I. Bjurhager, L. Rautkari, E.K. Gamstedt, The influence of chemical degradation and polyethylene glycol on moisture-dependent cell wall properties of archeological wooden objects: a case study of the Vasa shipwreck, Wood Sci. Technol. 50 (2016) 1103–1123, doi:10.1007/s00226-016-0861-x.
[10] J. Preston, A.D. Smith, E.J. Schofield, A.V. Chadwick, M.A. Jones, J.E.M. Watts, The effects of mary rose conservation treatment on iron oxidation processes and microbial communities contributing to acid production in marine archaeological timbers, PLoS One 9 (2014) e84169, doi:10.1371/journal.pone.0084169.
[11] H. Collett, F. Bouville, F. Giuliani, E. Schofield, Structural monitoring of a large archaeological wooden structure in real time, post PEG treatment, Forests 12 (2021) 1788, doi:10.3390/f12121788.
[12] P. Hoffmann, K. Choi, Y. Kim, The 14th-century Shinan ship—progress in conservation, Int. J. Nautical Archaeol. (1991) https://www.tandfonline.com/doi/abs/10.1111/j.1095-9270.1991.tb00297.x. (accessed March 21, 2024).
[13] A. Tahira, W. Howard, E.R. Pennington, A. Kennedy, Mechanical strength studies on degraded waterlogged wood treated with sugars, Stud. Conserv. 62 (2017) 223–228, doi:10.1080/00393630.2016.1169364.
[14] A. Kennedy, E.R. Pennington, Conservation of chemically degraded waterlogged wood with sugars, Stud. Conserv. 59 (2014) 194–201, doi:10.1179/2047058413Y.0000000109.
[15] F. Antonelli, G. Galotta, G. Sidoti, F. Zikeli, R. Nisi, B.D. Petriaggi, M. Romagnoli, Cellulose and lignin nano-scale consolidants for waterlogged archaeological wood, Front. Chem. 8 (2020), doi:10.3389/fchem.2020.00032.
[16] J. Zhang, Y. Li, D. Ke, C. Wang, H. Pan, K. Chen, H. Zhang, Modified lignin nanoparticles as potential conservation materials for waterlogged archaeological wood, ACS Appl. Nano Mater. 6 (2023) 12351–12363, doi:10.1021/acsanm.3c01998.
[17] Z. Walsh, E.-R. Janeček, M. Jones, O.A. Scherman, Natural polymers as alternative consolidants for the preservation of waterlogged archaeological wood, Stud. Conserv. 62 (2017) 173–183, doi:10.1179/2047058414Y.0000000149.
[18] E. McHale, S. Braovac, C.C. Steindal, R.B. Gillis, G.G. Adams, S.E. Harding, T. Benneche, H. Kutzke, Synthesis and characterisation of lignin-like oligomers as a bio-inspired consolidant for waterlogged archaeological wood, Pure Appl. Chem. 88 (2016) 969–977, doi:10.1515/pac-2016-0814.
[19] Y. Hu, X. Wang, L. Liu, B. Zhang, L. Jiang, Preparation of bacterial cellulose for xylitol-reinforced waterlogged wood, Archaeometry 66 (2024) 618–632, doi:10.1111/arcm.12958.
[20] M. Christensen, E. Larnøy, H. Kutzke, F.K. Hansen, Treatment of waterlogged archaeological wood using chitosan-and modified chitosan solutions. Part 1: chemical compatibility and microstructure, J. Am. Inst. Conserv. 54 (2015) 3–13, doi:10.1179/1945233014Y.0000000034.
[21] F. Parisi, F. Bernardini, G. Cavallaro, L. Mancini, S. Milioto, D. Prokop, G. Lazzara, Halloysite nanotubes/pluronic nanocomposites for waterlogged archeological wood: thermal stability and X-ray microtomography, J. Therm. Anal. Calorim. 141 (2020) 981–989, doi:10.1007/s10973-020-09637-4.
[22] G. Cavallaro, G. Lazzara, S. Milioto, F. Parisi, V. Sparacino, Thermal and dynamic mechanical properties of beeswax-halloysite nanocomposites for consolidating waterlogged archaeological woods, Polym. Degr. Stabil. 120 (2015) 220–225, doi:10.1016/j.polymdegradstab.2015.07.007.
[23] G. Cavallaro, G. Lazzara, S. Milioto, F. Parisi, F. Ruisi, Nanocomposites based on esterified colophony and halloysite clay nanotubes as consolidants for waterlogged archaeological woods, Cellulose 24 (2017) 3367–3376, doi:10.1007/s10570-017-1369-8.
[24] L. Lisuzzo, T. Hueckel, G. Cavallaro, S. Sacanna, G. Lazzara, Pickering emulsions based on wax and halloysite nanotubes: an ecofriendly protocol for the treatment of archeological woods, ACS Appl. Mater. Interfaces. (2020), doi:10.1021/acsami.0c20443.
[25] Y. Kawahara, P. ENDO, T. Kimura, Conservation treatment for archaeological waterlogged woods using keratin from waste down, J. Text. Eng. 48 (2002) 107–110, doi:10.4188/jte.48.107.
[26] R. Endo, K. Kamei, I. Iida, M. Yokoyama, Y. Kawahara, Physical and mechanical properties of waterlogged wood treated with hydrolyzed feather keratin, J. Archaeol. Sci. 37 (2010) 1311–1316, doi:10.1016/j.jas.2009.12.034.
[27] R. Endo, J. Sugiyama, Evaluation of cell wall reinforcement in feather keratin-treated waterlogged wood as imaged by synchrotron X-ray microtomography (μXRT) and TEM, Holzforschung 67 (2013) 795–803, doi:10.1515/hf-2012-0181.
[28] R. Endo, J. Sugiyama, New attempts with the keratin-metal/magnesium process for the conservation of archaeological waterlogged wood, J. Cult. Herit. 54 (2022) 53–58, doi:10.1016/j.culher.2022.01.002.
[29] S. Li, Y. Zeng, L. Zhou, N. Feng, C. Li, L. Sheng, Y. Li, J. Sun, Consolidation of waterlogged archaeological woods by reversibly cross-linked polymers, J. Archaeol. Sci.: Reports 57 (2024) 104675, doi:10.1016/j.jasrep.2024.104675.
[30] Y. Zhou, Y. Zhang, L. Kan, Y. Wang, K. Wang, D. Hu, Aqueous modification of waterlogged archaeological wood by phenylboronic acid to reduce hygroscopicity and improve the dimensional stability, Wood. Sci. Technol. 58 (2024) 941–957, doi:10.1007/s00226-024-01551-4.
[31] Y. Zhou, Y. Zhang, K. Wang, D. Hu, Well-controlled SI-ARGET ATRP of EGDMA for maintaining the dimensions of waterlogged archaeological wood, Wood Sci. Technol. 57 (2023) 523–535, doi:10.1007/s00226-023-01454-w.
[32] Q. Huang, J. Zha, X. Han, H. Wang, Temporary consolidation of marine artifact based on polyvinyl alcohol/tannic acid reversible hydrogel, Polymers 15 (2023) 4621, doi:10.3390/polym15244621.
[33] X. Wang, H. Wang, B. Zhang, Y. Hu, L. Zhu, Temporary solidification and extraction of marine archaeological wood underwater at a depth of seven meters: a further contribution, J. Cult. Herit. 62 (2023) 13–20, doi:10.1016/j.culher.2023.05.012.
[34] Y. Wang, X. Wang, W. Chen, L. Zhu, B. Zhang, Environmental stimulant-responsive hydrogels based on polyethylene glycol-derived polymer for underwater bonding and extraction of fragile wooden relics: synthesis, characterization, and preliminary application, Int. J. Adh. Adh. 131 (2024) 103651, doi:10.1016/j.ijadhadh.2024.103651.
[35] Y. Zhou, K. Wang, D. Hu, High retreatability and dimensional stability of polymer grafted waterlogged archaeological wood achieved by ARGET ATRP, Sci. Rep. 9 (2019) 1–9, doi:10.1038/s41598-019-46366-7.

[36] Y. Zhou, K. Wang, D. Hu, Surface-initiated ARGET ATRP for maintaining the dimension of waterlogged archaeological wood (Pinus massoniana): polymer distribution behaviors and anti-shrinkage mechanism, Wood. Sci. Technol. 56 (2022) 205–218, doi:10.1007/s00226-021-01342-1.
[37] Y. Zhou, K. Wang, D. Hu, An aqueous approach to functionalize waterlogged archaeological wood followed by improved surface-initiated ARGET ATRP for maintaining dimensional stability, Cellulose 28 (2021) 2433–2443, doi:10.1007/s10570-020-03664-y.
[38] M. Broda, B. Mazela, A. Dutkiewicz, Organosilicon compounds with various active groups as consolidants for the preservation of waterlogged archaeological wood, J. Cult. Herit. 35 (2019) 123–128, doi:10.1016/j.culher.2018.06.006.
[39] M. Broda, B. Mazela, K. Radka, Methyltrimethoxysilane as a stabilising agent for archaeological waterlogged wood differing in the degree of degradation, J. Cult. Herit. 35 (2019) 129–139, doi:10.1016/j.culher.2018.06.004.
[40] M. Broda, D.J. Yelle, Reactivity of waterlogged archeological elm wood with organosilicon compounds applied as wood consolidants: 2D 1H–13C solution-state NMR studies, Molecules 27 (2022) 3407, doi:10.3390/molecules27113407.
[41] M. Broda, J.E. Jakes, L. Li, O.A. Antipova, Archeological wood conservation with selected organosilicon compounds studied by XFM and nanoindentation, Wood Sci. Technol. 57 (2023) 1277–1298, doi:10.1007/s00226-023-01503-4.
[42] M. Broda, S.F. Curling, M.J. Spear, C.A.S. Hill, Effect of methyltrimethoxysilane impregnation on the cell wall porosity and water vapour sorption of archaeological waterlogged oak, Wood Sci. Technol. 53 (2019) 703–726, doi:10.1007/s00226-019-01095-y.
[43] M. Broda, J.E. Jakes, L. Li, O.A. Antipova, E.R. Maxey, Q. Jin, Conservation of model degraded pine wood with selected organosilicons studied by XFM and nanoindentation, Wood Sci. Technol. 58 (2024) 649–675, doi:10.1007/s00226-024-01533-6.
[44] C.-M. Popescu, M. Broda, Interactions between different organosilicons and archaeological waterlogged wood evaluated by infrared spectroscopy, Forests 12 (2021) 268, doi:10.3390/f12030268.
[45] M. Broda, M.J. Spear, S.F. Curling, G.A. Ormondroyd, The viscoelastic behaviour of waterlogged archaeological wood treated with methyltrimethoxysilane, Materials 14 (2021) 5150, doi:10.3390/ma14185150.
[46] P.A. Penttilä, L. Rautkari, M. Österberg, R. Schweins, Small-angle scattering model for efficient characterization of wood nanostructure and moisture behaviour, J. Appl. Cryst. 52 (2019) 369–377, doi:10.1107/S1600576719002012.
[47] M. Martínez-Sanz, M.J. Gidley, E.P. Gilbert, Application of X-ray and neutron small angle scattering techniques to study the hierarchical structure of plant cell walls: a review, Carbohydr. Polym. 125 (2015) 120–134, doi:10.1016/j.carbpol.2015.02.010.
[48] P.A. Penttilä, M. Altgen, N. Carl, P. van der Linden, I. Morfin, M. Österberg, R. Schweins, L. Rautkari, Moisture-related changes in the nanostructure of woods studied with X-ray and neutron scattering, Cellulose 27 (2020) 71–87, doi:10.1007/s10570-019-02781-7.
[49] P.A. Penttilä, M. Altgen, M. Awais, M. Österberg, L. Rautkari, R. Schweins, Bundling of cellulose microfibrils in native and polyethylene glycol-containing wood cell walls revealed by small-angle neutron scattering, Sci. Rep. 10 (2020) 1–9, doi:10.1038/s41598-020-77755-y.
[50] L.H. Thomas, A. Martel, I. Grillo, M.C. Jarvis, Hemicellulose binding and the spacing of cellulose microfibrils in spruce wood, Cellulose 27 (2020) 4249–4254, doi:10.1007/s10570-020-03091-z.
[51] N.Z. Plaza, S.V. Pingali, S. Qian, W.T. Heller, J.E. Jakes, Informing the improvement of forest products durability using small angle neutron scattering, Cellulose 23 (2016) 1593–1607, doi:10.1007/s10570-016-0933-y.
[52] A.N. Fernandes, L.H. Thomas, C.M. Altaner, P. Callow, V.T. Forsyth, D.C. Apperley, C.J. Kennedy, M.C. Jarvis, Nanostructure of cellulose microfibrils in spruce wood, PNAS 108 (2011) E1195–E1203, doi:10.1073/pnas.1108942108.
[53] L.H. Thomas, V.T. Forsyth, A. Martel, I. Grillo, C.M. Altaner, M.C. Jarvis, Structure and spacing of cellulose microfibrils in woody cell walls of dicots, Cellulose 21 (2014) 3887–3895, doi:10.1007/s10570-014-0431-z.
[54] A. Zitting, A. Paajanen, L. Rautkari, P.A. Penttilä, Deswelling of microfibril bundles in drying wood studied by small-angle neutron scattering and molecular dynamics, Cellulose 28 (2021) 10765–10776, doi:10.1007/s10570-021-04204-y.
[55] N.Z. Plaza, J.E. Jakes, C.R. Frihart, C.G. Hunt, D.J. Yelle, L.F. Lorenz, W.T. Heller, S.V. Pingali, D.S. Stone, Small-angle neutron scattering as a new tool to evaluate moisture-induced swelling in the nanostructure of chemically modified wood cell walls*, For. Prod. J. 68 (2018) 349–352, doi:10.13073/FPJ-D-17-00065.
[56] P.A. Penttilä, A. Zitting, T. Lourençon, M. Altgen, R. Schweins, L. Rautkari, Water-accessibility of interfibrillar spaces in spruce wood cell walls, Cellulose 28 (2021) 11231–11245, doi:10.1007/s10570-021-04253-3.
[57] J. Guo, H. Rennhofer, Y. Yin, H.C. Lichtenegger, The influence of thermo-hygro-mechanical treatment on the micro- and nanoscale architecture of wood cell walls using small- and wide-angle X-ray scattering, Cellulose 23 (2016) 2325–2340, doi:10.1007/s10570-016-0982-2.
[58] K. Toba, H. Yamamoto, M. Yoshida, Crystallization of cellulose microfibrils in wood cell wall by repeated dry-and-wet treatment, using X-ray diffraction technique, Cellulose 20 (2013) 633–643, doi:10.1007/s10570-012-9853-7.
[59] N.Z. Plaza, S.V. Pingali, R.E. Ibach, Nanostructural changes correlated to decay resistance of chemically modified wood fibers, Fibers 10 (2022) 40, doi:10.3390/fib10050040.
[60] P. Chen, Y. Li, Y. Nishiyama, S.V. Pingali, H.M. O'Neill, Q. Zhang, L.A. Berglund, Small angle neutron scattering shows nanoscale PMMA distribution in transparent wood biocomposites, Nano Lett. 21 (2021) 2883–2890, doi:10.1021/acs.nanolett.0c05038.
[61] K. Svedström, I. Bjurhager, A. Kallonen, M. Peura, R. Serimaa, Structure of oak wood from the Swedish warship Vasa revealed by X-ray scattering and microtomography, Holzforschung 66 (2012) 355–363, doi:10.1515/hf.2011.157.
[62] J. Guo, J. Chen, Q. Meng, L. Ploszczanski, J. Liu, R. Luo, T. Jin, P. Siedlaczek, H.C. Lichtenegger, Y. Yin, H. Rennhofer, Molecular and crystal structures of cellulose in severely deteriorated archaeological wood, Cellulose 29 (2022) 9549–9568, doi:10.1007/s10570-022-04856-4.
[63] L. Han, X. Tian, T. Keplinger, H. Zhou, R. Li, K. Svedström, I. Burgert, Y. Yin, J. Guo, Even visually intact cell walls in waterlogged archaeological wood are chemically deteriorated and mechanically fragile: a case of a 170 year-old shipwreck, Molecules 25 (2020) 1113, doi:10.3390/molecules25051113.
[64] A. Stempin, The early piast settlement on Ostrów Tumski (Cathedral Island) in Poznań–the popularisation of heritage from the standpoint of the Genius Loci Archaeological Reserve, Analecta Archaeologica Ressoviensia 13 (2018) 275–286.
[65] M. Broda, C.-M. Popescu, Natural decay of archaeological oak wood versus artificial degradation processes—an FT-IR spectroscopy and X-ray diffraction study, Spectrochim. Acta A-M 209 (2019) 280–287, doi:10.1016/j.saa.2018.10.057.
[66] M. Broda, N.Z. Plaza, J.E. Jakes, C. Baez, S.V. Pingali, W. Bras, Effect of alkali treatment and fungal degradation on the nanostructure and cellulose arrangement in Scots pine cell walls – a neutron and X-ray scattering study, Carbohydr. Polym. 347 (2025) 122733, doi:10.1016/j.carbpol.2024.122733.
[67] W.T. Heller, V.S. Urban, G.W. Lynn, K.L. Weiss, H.M. O'Neill, S.V. Pingali, S. Qian, K.C. Littrell, Y.B. Melnichenko, M.V. Buchanan, D.L. Selby, G.D. Wignall, P.D. Butler, D.A. Myles, The bio-SANS instrument at the high flux isotope reactor of Oak Ridge National Laboratory, J. Appl. Cryst. 47 (2014) 1238–1246, doi:10.1107/S1600576714011285.
[68] W.T. Heller, J. Hetrick, J. Bilheux, J.M.B. Calvo, W.-R. Chen, L. DeBeer-Schmitt, C. Do, M. Doucet, M.R. Fitzsimmons, W.F. Godoy, G.E. Granroth, S. Hahn, L. He, F. Islam, J. Lin, K.C. Littrell, M. McDonnell, J. McGaha, P.F. Peterson, S.V. Pingali, S. Qian, A.T. Savici, Y. Shang, C.B. Stanley, V.S. Urban, R.E. Whitfield, C. Zhang, W. Zhou, J.J. Billings, M.J. Cuneo, R.M.F. Leal, T. Wang, B. Wu, drtsans: the data reduction toolkit for small-angle neutron scattering at Oak Ridge National Laboratory, SoftwareX 19 (2022) 101101, doi:10.1016/j.softx.2022.101101.
[69] J. Ilavsky, P.R. Jemian, Irena: tool suite for modeling and analysis of small-angle scattering, J. Appl. Cryst. 42 (2009) 347–353, doi:10.1107/S0021889809002222.
[70] J. Ilavsky, Nika: software for two-dimensional data reduction, J. Appl. Cryst. 45 (2012) 324–328, doi:10.1107/S0021889812004037.
[71] H.F. Jakob, D. Fengel, S.E. Tschegg, P. Fratzl, The elementary cellulose fibril in Picea abies: comparison of transmission electron microscopy, small-angle X-ray scattering, and wide-angle X-ray scattering results, Macromolecules 28 (1995) 8782–8787, doi:10.1021/ma00130a010.
[72] M. Newville, T. Stensitzki, D.B. Allen, A. Ingargiola, LMFIT: non-linear least-square minimization and curve-fitting for python, (2014). https://doi.org/10.5281/zenodo.11813.
[73] D. Fernando, M. Kowalczyk, P. Guindos, M. Auer, G. Daniel, Electron tomography unravels new insights into fiber cell wall nanostructure; exploring 3D macromolecular biopolymeric nano-architecture of spruce fiber secondary walls, Sci. Rep. 13 (2023) 2350, doi:10.1038/s41598-023-29113-x.
[74] P. Xu, L.A. Donaldson, Z.R. Gergely, L.A. Staehelin, Dual-axis electron tomography: a new approach for investigating the spatial organization of wood cellulose microfibrils, Wood. Sci. Technol. 41 (2007) 101–116, doi:10.1007/s00226-006-0088-3.
[75] Y.Z. Zhang, X.L. Chen, J. Liu, P.J. Gao, D.X. Shi, S.J. Pang, Size and arrangement of elementary fibrils in crystalline cellulose studied with scanning tunneling microscopy, J. Vacuum Sci. Technol. B: Microelectron. Nanometer Struct. Process., Meas., Phenomena 15 (1997) 1502–1505, doi:10.1116/1.589483.
[76] A.N.J. Heyn, The elementary fibril and supermolecular structure of cellulose in soft wood fiber, J. Ultrastruct. Res. 26 (1969) 52–68, doi:10.1016/S0022-5320(69)90035-5.
[77] Y. Wei, M.J.A. Hore, Characterizing polymer structure with small-angle neutron scattering: a Tutorial, J. Appl. Phys. 129 (2021) 171101, doi:10.1063/5.0045841.
[78] R.E. Ibach, N.Z. Plaza, S.V. Pingali, Small angle neutron scattering reveals wood nanostructural features in decay resistant chemically modified wood, Front. For. Glob. Change 4 (2022) 1–11, doi:10.3389/ffgc.2021.814086.
[79] A. García-Iruela, L. García Esteban, F. García Fernández, P. de Palacios, A.B. Rodriguez-Navarro, L.G. Sánchez, R. Hosseinpourpia, Effect of degradation on wood hygroscopicity: the case of a 400-year-old coffin, Forests 11 (2020) 712, doi:10.3390/f11070712.
[80] G. Giachi, F. Bettazzi, S. Chimichi, G. Staccioli, Chemical characterisation of degraded wood in ships discovered in a recent excavation of the Etruscan and Roman harbour of Pisa, J. Cult. Herit. 4 (2003) 75–83, doi:10.1016/S1296-2074(03)00018-9.
[81] N. Hayeemasae, A. Adair, S. Soontaranon, M.S. Mohamad Rasidi, A. Masa, Optimising silane coupling agent content in phenolic-resin-cured sepiolite-filled natural rubber composites, J. Rubber Res. (2023), doi:10.1007/s42464-023-00210-w.
[82] P. Sae-oui, C. Sirisinha, U. Thepsuwan, K. Hatthapanit, Roles of silane coupling agents on properties of silica-filled polychloroprene, Eur. Polym. J. 42 (2006) 479–486, doi:10.1016/j.eurpolymj.2005.09.003.